Geotech Geol Eng (2024) 42:3171–3191
https://doi.org/10.1007/s10706-023-02723-y

ORIGINAL PAPER

An Experimental Study on the Lateral Behavior of Piles in Unsaturated Sand Under Monotonic, Cyclic and Post Cyclic Loading

Roozbeh Owji · Ghassem Habibagahi · Mehdi Veiskarami

Received: 14 April 2023 / Accepted: 8 December 2023 / Published online: 21 January 2024

Abstract Piles supporting large structures are often subjected to cyclic lateral loads due to natural phenomena, including earthquakes, winds, and waves. Such loads are main causes of progressive deterioration in the stiffness and reduce the lateral capacity of piles. However, the effects of unsaturated soil conditions on the lateral cyclic response of piles are not yet fully understood, and the p–y curves used in engineering practice are merely based on the assumption of full saturation or complete dry conditions. This study is aimed to investigate the pile performance under unsaturated soil conditions by performing monotonic, cyclic, and post-cyclic loading tests on piles installed in sand with a varying water table. A loading system was designed and constructed to carry out different types of cyclic loadings. It was observed that the lateral capacity of the pile is influenced by the average suction stress along the pile which increases with the depth of the water table. During the cyclic loading, gap formation is noticed around the pile head for tests conducted in unsaturated conditions, which results in significant stiffness degradation compared to the saturated state. However, post-cyclic loading tests showed that the ultimate lateral capacity of the pile is not affected by the cyclic loading history. Finally, a modified p–y curve is proposed for the piles embedded in unsaturated sandy soils, and a comparison of its performance with the observed results is promising.

Keywords Cyclic loading · p–y curve · Pile · Lateral loading · Unsaturated soil

Supplementary Information The online version contains supplementary material available at https://doi.org/10.1007/s10706-023-02723-y.

R. Owji · G. Habibagahi · M. Veiskarami (✉)
School of Engineering, Shiraz University, Shiraz, Iran
e-mail: mveiskarami@shirazu.ac.ir

R. Owji
e-mail: roozbeh_73@yahoo.com

G. Habibagahi
e-mail: habibg@shirazu.ac.ir

1 Introduction

One of the most important concerns in the design of pile foundations is their behavior and performance under lateral cyclic loads (Basack 2015; Basack and Dey 2012). Cyclic loads are caused by environmental effects, namely, earthquakes, wind, and waves, which can occur in the foundations of wind turbines and high-rise structures (Long and Vanneste 1994; Rathod et al. 2020). Based on the direction of the loads acted on piles, lateral cyclic loads can be classified into one-way and two-way loading, which may be applied under load-controlled or displacement-controlled conditions (Basack and Purkayastha 2007; Consoli et al. 2023). In the case of two-way loading, the piles can experience symmetric or asymmetric loads depending on the nature of the applied cyclic loads. Nevertheless, there are major differences between the one-way and the two-way cyclic loading. Some researchers reported that one-way cyclic loading can lead to greater stiffness reduction and displacement accumulation (Darvishi Alamouti et al. 2019; He et al. 2017; Long and Vanneste 1994). On the opposite, Arshad and O'Kelly (2014) found that an increase in rotation under two-way loading was remarkably greater than that of one-way loading. Also, other studies showed that the highest degradation in the stiffness, occurred at asymmetric two-way loading due to lower particle densification near the pile (Frick and Achmus 2020; LeBlanc et al. 2010). However, controversial results have been reported in the literature.

The most common method in engineering practice for the design of piles under lateral loads is the p–y curves which are proposed in the American Petroleum Institute (API) recommendations (API 2000). However, a limitation of the API p–y curve for sandy soils is its prediction of cyclic lateral response by simply multiplying the static p–y curve at all depths by an empirical correction factor (i.e., 0.9). Thieken et al. (2015) proposed a modification for the API p–y curve in the case of cyclic loading in which the number of load cycles were incorporated into the model. Due to the complex nonlinear characteristics of soil and the damping effect on energy dissipation, cyclic p–y models have rarely been reported. In addition to these works, interested readers may also refer to the works of (Cheng et al. 2022; Choi et al. 2015; Wang and Liu 2016). The response of pile under cyclic loading is highly dependent on properties of the cyclic loading, including the number of cycles, frequency, and cyclic load ratio (Long and Vanneste 1994; Chandrasekaran et al. 2010; Arshad and O'Kelly 2014; Basack and Nimbalkar 2018; Owji et al. 2023). These studies have mainly focused on fully saturated or completely dry soil conditions, and no consideration has been given to soils in their unsaturated condition. In arid and semi-arid areas, where the water table is not close to the ground surface, a significant portion of the pile length is embedded in the unsaturated zone within which the degree of saturation varies with depth.

It is well known that the behavior of partially saturated soils is different from that of saturated soils. The reason is the variation of the soil stiffness which is influenced by the soil matric suction (Lu and Likos 2006; Oh and Vanapalli 2013). Al-Khazaali and Vanapalli (2019) demonstrated that the contribution of matric suction to the axial capacity of piles could result in 2–2.5 times higher axial capacity compared to the saturated condition. On the other hand, the p–y curve and hysteretic behavior of pile during cyclic lateral loading are substantially governed by the relative stiffness of the soil-pile system (Choo and Kim 2016; Komolafe and Ghayoomi 2023), and thus the effects of matric suction on soil-pile interaction during cycling will be complex.

Physical model tests are needed to understand the influence of the degree of saturation on the lateral capacity of piles under both cyclic and monotonic loading. However, there are only a few experimental works addressing the effects of the degree of saturation on the lateral behavior of piles in Centrifuge (Machmer 2012; Lalicata et al. 2019) as well as conventional tests (Awad-Allah et al. 2017) which are briefly explained. Machmer (2012) evaluated lateral pile response in unsaturated soil under static and earthquake loading using centrifuge modelling. Static test results showed that the pile bending moment in unsaturated conditions was larger than in dry condition. Under dynamic loading, pile settlement for unsaturated conditions significantly reduced compared to the dry state. Subsequently, the influence of partial saturation of sand on the performance of piles under two-way cyclic loading was studied by Awad-Allah et al. (2017). In this research, the behavior of pile embedded in dense dry sand was compared with the results observed from the tests carried out under similar conditions but with a uniform degree of saturation of 86%. The comparison showed that in the dry case, the modulus of subgrade reaction increased with the number of load cycles, while a significant reduction was observed under the unsaturated condition. More recently, Lalicata et al. (2019) conducted centrifuge model tests on a rigid pile in unsaturated silty soil with two different water table levels; one located at the soil surface and another at the half pile length. They concluded that partial saturation caused improvement in the lateral pile capacity, and comparing the loose and dense states, this improvement was more pronounced for the loose state. However, in the first study, the measured degree of saturation along the pile length was completely different from real conditions (and hence, results cannot represent the actual pile-soil response). In the second study, the contribution of matric suction to the lateral capacity of the pile was very negligible (degree of saturation,

S_r = 86%), failing to accurately demonstrate the influence of partial saturation on the pile response. In the last attempt, there was no consideration for a partially saturated condition.

Soils in arid and semi-arid climates often appear in an unsaturated state, which significantly impacts their mechanical properties. Consequently, the soil-structure interaction is influenced by the matric suction experienced within these soils. However, previous researches have overlooked the impact of partial saturation on pile behavior, mainly due to the scarcity of large scale in-situ investigation and sophisticated laboratory experiments. The review of previous works stated above indicates that the role of the degree of saturation on the behavior of piles under lateral cyclic loading has not been well investigated. There is still a considerable lack of knowledge about the influence of cyclic loading direction, especially in unsaturated conditions. Therefore, a comprehensive study is required to identify the combined effects of the two issues on the p–y curves. Moreover, most previous studies have focused on the lateral behavior of rigid piles, and less attention has yet been given to flexible piles. In this study, a physical model representing a flexible pile is subjected to a series of cyclic and monotonic lateral loading under saturated and unsaturated soil conditions which are commonly encountered in engineering design. The main objectives and novelty of the present work, therefore, lie in: (a) investigation of the effect of variable partial saturation with depth (analogous to the field condition); (b) examining the pile behavior under different types of lateral cyclic loadings covering one-way as well as symmetric and asymmetric two-way loadings; (c) understanding the effects of cyclic loading on the ultimate lateral capacity by performing post-cyclic loading tests; (d) development of a modified p–y curve for such conditions. To meet all these goals, an extensive experimental program was carried out with details presented in the following sections.

2 Materials and Methods

2.1 Model Pile

A single stainless steel pipe with an outer diameter of 25 mm, a wall thickness of 0.6 mm, and an embedded length of 550 mm, was employed in this study. The elastic Young's modulus and the yield bending moment of the model pile are 197 GPa and 90 Nm, respectively. The relative stiffness of the pile-soil system was determined according to the Broms (1964a, b) and Poulos and Hull (1989) equations which indicate that the lateral pile behavior is close to the flexible pile. Dietrich (1982) reported that while the behavior of rigid pile is significantly influenced by the pile aspect ratio (i.e. the ratio of the embedded length to the diameter), the behavior of flexible pile is affected mainly by the bending stiffness.

Every small-scale test must take into account some scaling considerations. Therefore, dimensions must be scaled so as to represent the expected pile behavior in the large-scale field condition. The model pile was scaled into the prototype pile using the similitude law proposed by Wood et al. (2002), given by:

$$\frac{E_m I_m}{E_n I_n} = \frac{1}{F^{4.5}} \tag{1}$$

where E_m, E_n, I_m, and I_n are the elastic moduli and moment of inertia of model and prototype pile, respectively, and F stands for the scale factor for the length. According to the above scaling law, the adopted model pile is equivalent to a steel pipe pile with an outer diameter of 0.7 m and an embedded length of 12.5 m. For an assumed prototype steel pile, the scaling factor is equal to 22.7. A summary of scaling procedure for the model and prototype piles are presented in Table 1.

2.2 Soil Properties

The soil used in this research is a uniform silica sand, classified as SP based on the Unified Soil

Table 1 Specifications of prototype pile and model pile

Property	Prototype pile	Model pile
Physical quantity	Steel ST37	Stainless steel
Embedded length of pile (m)	12.5	0.55
Pile diameter (m)	0.7	0.025
Elastic modulus of pile (GPa)	210	197
Bending stiffness of pile (kN m^2)	8.48×10^5	0.72
Elastic modulus of soil (MPa)	25	6
Relative stiffness	0.001	0.001

Classification System (ASTM D2487-00) with the grain size distribution curve shown in Fig. 1. As a well-known construction material in many regions of Iran, this soil has been obtained from Firoozkooh in Tehran province, Iran. The particle size distribution of the sand used in this research is very similar to the sand used by previous researchers (Al-Khazaali and Vanapalli 2019; Awad-Allah et al. 2017). The ratio of pile diameter (25 mm) to the mean grain size (0.18 mm) is approximately 139, ensuring the elimination of particle size effects on the results. Klinkvort et al. (2013) suggested a ratio of more than 50 would be adequate to prevent the scale effect.

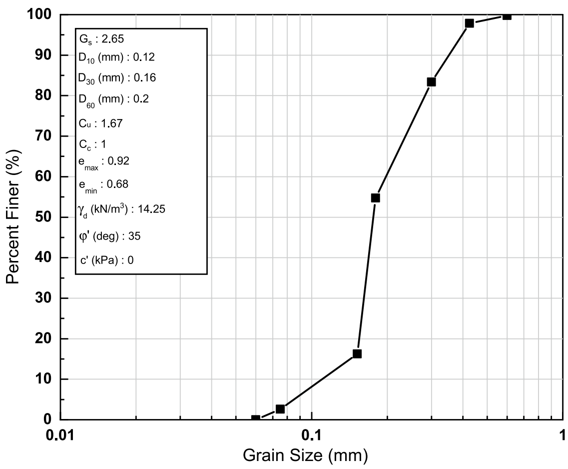

Fig. 1 Grain size distribution curve of tested sand

2.3 Water Retention Test

Soil water retention curve (SWRC) was obtained from the hanging column test according to ASTM D6836 (ASTM 2008), commonly used for SWRC measurement in coarse-grained soils. For this purpose, a hanging column setup (HCS) was fabricated in the laboratory, illustrated in Fig. 2. Testing apparatuses for HCS included a testing cell with an internal diameter of 64 mm and height of 45 mm, ceramic disk with an air entry value of 80 kPa, upper reservoir, lower reservoir (i.e., adjustable reservoir), capillary tube, and vacuum gauge as shown in Fig. 2a. Sand was placed in the cell and tamped to reach the

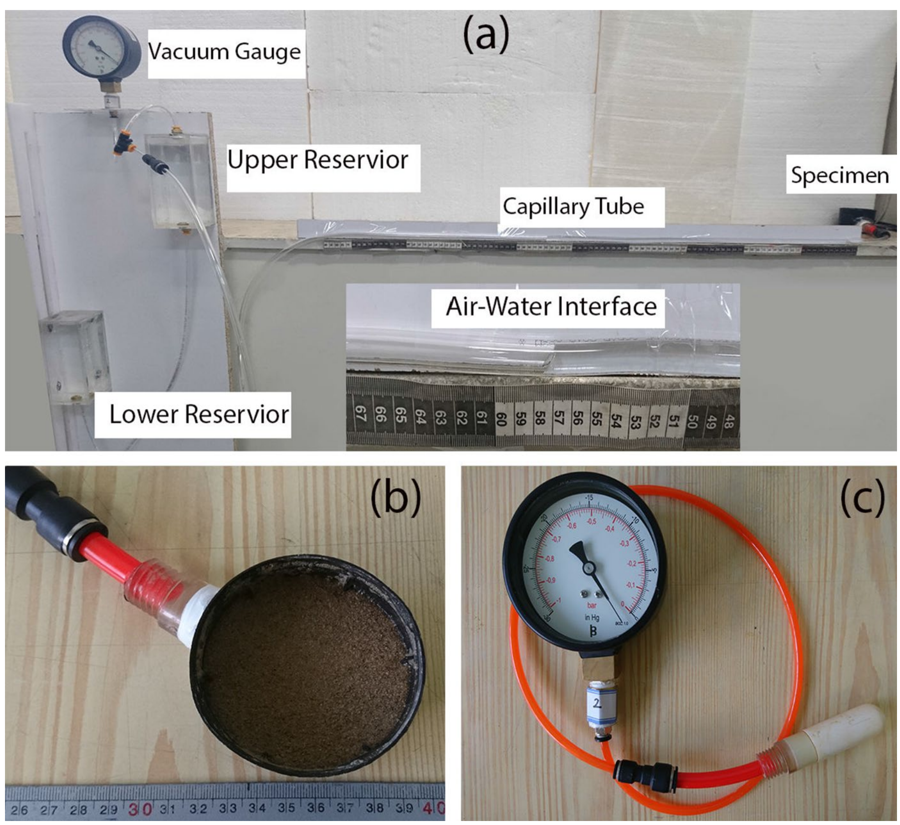

Fig. 2 Test setup for measuring SWRC: **a** hanging column setup; **b** soil specimen; **c** mini-tensiometer

target density (i.e., density index of 40%) (Fig. 2b). After saturating the sample from the bottom line, the sample was allowed to reach the equilibrium state for at least 24 h, and then the final location of the air–water interface in the capillary tube was measured accurately. Elevation of the upper reservoir was maintained constant, and then elevation of the regulating reservoir was lowered until the vacuum gauge showed the desired suction. After equilibrium, the new position of the air–water interface corresponding to the end of the applied matric suction was recorded. This procedure was repeated by increasing the applied suction to cover the whole range of suction values required to develop the SWRC. The measured data points were then utilized to generate a continuous soil water retention curve using the van Genuchten (VG) model (Van Genuchten 1980):

$$S_e = \left[\frac{1}{1 + B(\psi)^n}\right]^m \tag{2}$$

where ψ is the matric suction and S_e shows the effective degree of saturation calculated as follows:

$$S_e = \frac{S - S_r}{1 - S_r} \tag{3}$$

and S_r is residual saturation. B, m, and n are fitting parameters of the VG model, which were optimized to the best fit to all SWRC data points. The obtained SWRC curve fitted with the VG model is shown in Fig. 3. From this figure, the air entry value of the sand was determined to be approximately equal to 2 kPa, and the degree of saturation of the sand reaches its residual value at a matric suction of 3.5 kPa.

2.4 Soil Box

A 600×300×900 mm (in length, width, and height, respectively) sand box was constructed from steel plates with the front side made of transparent plexiglass of 15 mm thickness (Fig. 4). These dimensions were chosen based on the model pile diameter (D_p) to minimize the boundary effects. According to Khari et al. (2013) and Matlock (1970), the distance between the model pile and side walls should be greater than 7–10 pile diameter in the direction of the lateral loading and 2.5 pile diameter perpendicular to the loading plane. Moreover, the distance below the pile tip should be extended down to 6 pile diameter.

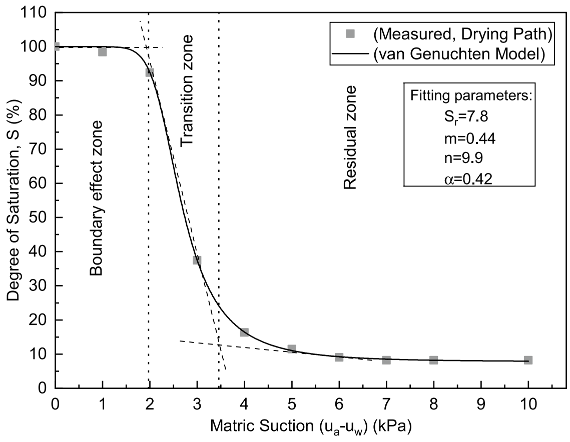

Fig. 3 SWRC of tested sand

Thus, the fabricated box is large enough to avoid any boundary effects on the obtained results. The wall thickness of the soil box was chosen 5 mm to make it practically rigid with no deflection during the pile loading tests.

A drainage layer consisting of 100 mm clean gravel with layers of geotextile was placed at the bottom of the soil box to allow a uniform flow of water in and out of the sand box. A water reservoir made of transparent plexiglass was connected to the drainage system of the soil box to supply a constant water table (WT) and to allow observation of the water level. Saturation and desaturation of the soil were facilitated using this mechanism. Once the water level reached the top of the soil surface, the water inflow was ceased by a float valve, and then the desired water table in the soil box was established by lowering the water level in the water reservoir. Details of the soil box and the loading device are depicted in Fig. 4. Direct measurement of matric suction was taken using a mini tensiometer as shown in Fig. 2c. As indicated in Fig. 4a, three mini-tensiometers were installed at depths of 0, 250, 450 mm to monitor the variation of matric suction with depth. Once the equilibrium was established, the matric suction readings were made on these gauges.

2.5 Loading System and Pile Instrumentation

A displacement control device has been designed and developed to apply both monotonic and cyclic lateral loading. The major components of this new

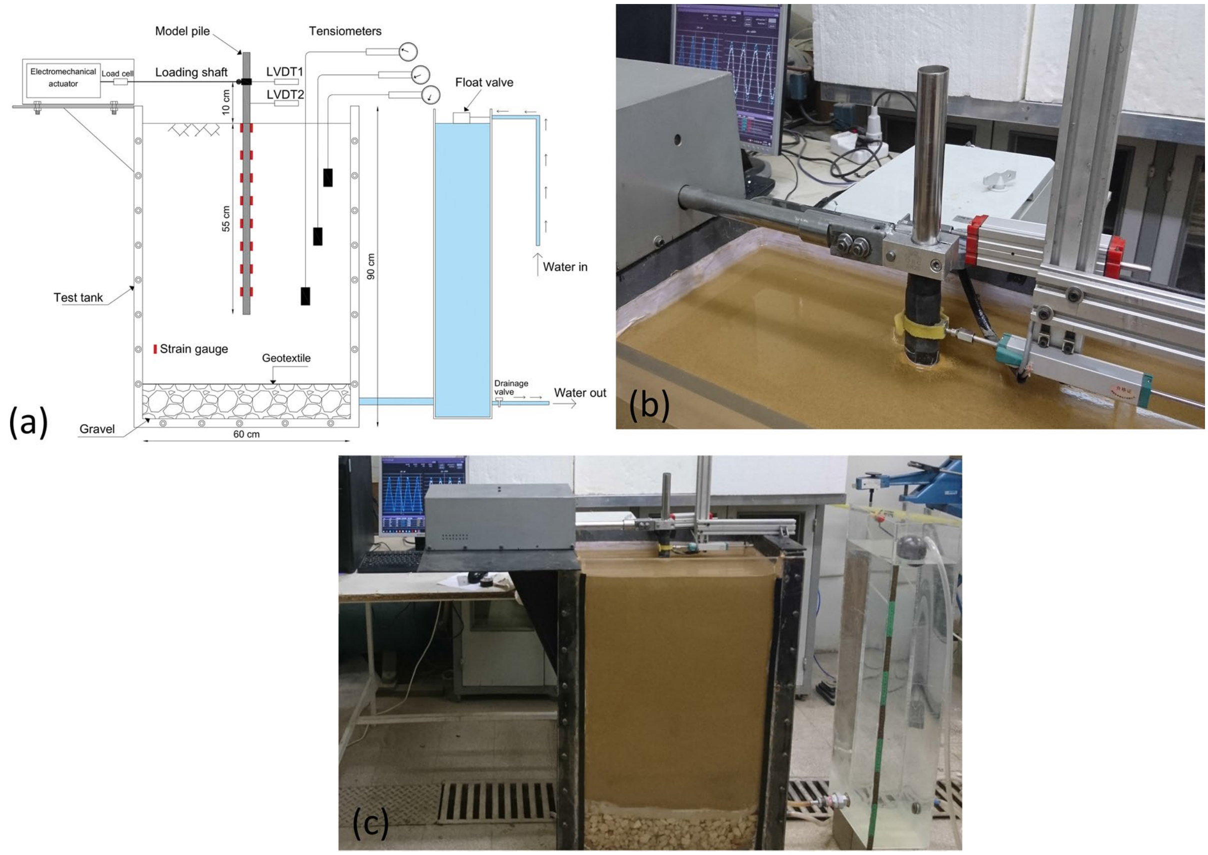

Fig. 4 Details of the experimental setup: **a** schematic of test setup and instrumentation; **b** cyclic loading system; **c** general arrangement

loading device are the stepper motor, ball screw, wagon, nut, and loading shaft. The stepper motor was programmed to generate sinusoidal displacements, allowing the control of various types of cyclic loading. The prominent advantage of the stepper motor is that it can control the position precisely and shows an excellent response to starting, stopping, and reversing. A hinge connection was placed between the loading shaft and pile head to enable free rotation around the pile axis; therefore, the moment at this point was assumed to be zero. In order to measure the force acting on the pile, a load cell with a capacity of 1.5 kN was placed between the loading shaft and wagon. Two linear variable differential transducers (LVDT) with a maximum displacement of 50 mm were also installed to the top portion of the pile (Fig. 4b). One LVDT was installed directly to the pile head, and another one was placed 30 mm above the soil surface. The latter LVDT measurements allowed the calculation of lateral displacement at the soil surface level, which is used as a boundary condition for the construction of p–y curves. To obtain a precise bending moment profile, eight strain gauge pairs with a half Wheatstone Bridge circuit configuration were attached on opposite sides of the pile surface and at equal intervals of 70 mm. Afterward, the pile shaft was covered with a heat shrink tube to protect strain gauges from water and possible damage during cyclic loading. The output data from the strain gauges, two LVDTs, and the load cell were collected and stored via a data acquisition system that displayed their values graphically on a computer screen. Computer software was developed to control and implement the lateral cyclic loading condition: the loading frequency, direction, amplitude, and the number of cycles. The arrangement of strain gauges, LVDTs, load cell, and loading device are presented in Fig. 4a and c.

2.6 Model Preparation

The interior sides of the soil box were marked with black and white strips and at intervals of 50 mm to effectively control the density of sand layers during preparation in the sand box. The moist sand was manually compacted in layers of 50 mm thickness to reach the target density index. Moreover, in certain tests, several containers were placed at varying elevations inside the soil box and weighted after the tests to check the soil density. In this study, tests were conducted on the sand with a density index of 40%. The behavior of sand is governed by the stress state. Dense sand may exhibit the behavior of loose sand under sufficiently high stress levels, while loose sand can behave similarly to dense one if the stress levels are quite low. Therefore, it is expected that the behavior of medium dense sand used in the lab to be similar to that of a dense sand under the field condition (Bolton 1986; Huang et al. 2015). Non-displacement pile installation was considered in this research. For this purpose, when the sand level reached the level corresponding to the pile tip, the pile was maintained vertically at the center of the sandbox and fixed from the top to the loading shaft. The sand was then compacted in layers until the appropriate embedded length was achieved. Experiments were performed under four different levels of the water table, including fully saturated (water table at the soil surface), 250 mm, 450 mm, and 750 mm below the soil surface. Unsaturated tests were conducted according to the method proposed by Al-Khazaali and Vanapalli (2019) with the following steps: (1) the compacted sand in the soil box was saturated from the bottom to push air bubbles to the surface. The submerged soil was kept for 24 h to ensure complete saturation condition; (2) water table was lowered to the specific depth and was left for another 24 h to reach the equilibrium condition. To prevent water evaporation from the sand surface throughout the test, the top of the soil box was completely wrapped with a plastic sheet. After reaching the equilibrium condition, suctions were measured, and the pile loading commenced. At the end of each test, soil samples were collected at different levels of the sand at intervals of 50 mm to obtain the variation of water content with depth. The laboratory testing program involved monotonic, cyclic, and post-cyclic lateral loading for a density index of 40%. To investigate the effects of cyclic load direction, four different conditions for the cyclic loading, namely, symmetric two-way, asymmetric two-way, one-way, and one-way without complete unloading were considered for the test program as depicted in Fig. 5. All cyclic loading tests were carried out up to 100 load cycles and with a frequency of 0.1 Hz and constant cyclic displacement amplitude of 3 mm, corresponding to $0.12D_p$. The reason for selecting a frequency of 0.1 Hz was that the predominant frequency in wind turbines is 0.1 Hz (Abadie 2015; Frick and Achmus 2020). The displacement amplitudes were chosen to reveal the Serviceability Limit State (SLS). Cyclic lateral loads for SLS in wind turbines are about 45–60% of the ultimate lateral capacity of the pile (LeBlanc et al. 2010). In order to evaluate the post-cyclic capacity, immediately after the cyclic phase, the pile was loaded monotonically the until pile head displacement reached $0.2D_p$. Results from the monotonic loading condition enabled measurement of the pile lateral bearing capacity under both saturated and unsaturated conditions. Finally, each loading test was repeated at least two times to ensure reproducibility of the test results.

3 Results and Discussion

3.1 Distribution of Degree of Saturation with Depth

The variation of the degree of saturation over the length of the pile in the equilibrium condition is

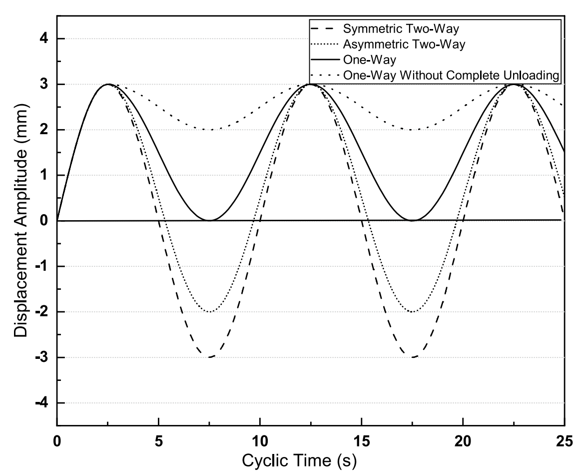

Fig. 5 Lateral cyclic displacement with various directions

shown in Fig. 6. The abbreviations Unsat1, Unsat2, and Unsat3 refer to the water table (WT) levels of 250 mm, 450 mm, and 750 mm, respectively. The degree of saturation in the region near the sand surface is similar in both Unsat2 and Unsat3 conditions, while Unsat1 is significantly different from the two. By lowering the WT from the ground surface, the matric suction gradually increases towards the soil surface and transfers from the boundary zone to the transition zone.

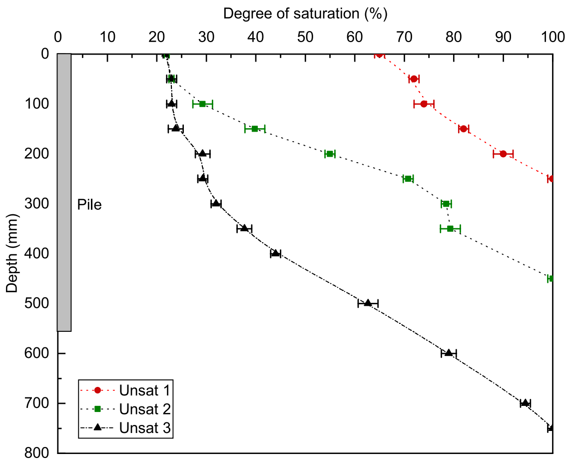

Fig. 6 Profiles of degree of saturation for unsaturated tests

3.2 Monotonic Loading

Figure 7a presents lateral load–displacement curves for monotonic loading tests in both saturated and unsaturated soils. The pile was monotonically loaded until the pile head displacement reached a limit of $0.2D_p$. In fact, $0.2D_p$ corresponds to the ultimate lateral load proposed by Broms (1964a, b). The lateral bearing capacity at any displacement level is substantially higher in tests with the soil in the unsaturated conditions. Raising the WT from 750 to 250 mm decreased the lateral capacity by 13%, and a further decrease in the WT depth from 250 mm to the soil surface led to a reduction in the lateral capacity by 42%. This result highlighted the significant role of the matric suction in the lateral pile response. Upon unloading, a considerable portion of the lateral displacement was recovered, about 75%, for the piles in unsaturated soil conditions and about 60% for the pile embedded in saturated soil. This finding shows that the suction stress significantly affects the elastic–plastic deformation of soil surrounding the pile. In general, suction enhances the ability of soil to recover its deformation by expanding the region of elastic deformation. That is, yielding and plastic deformation can occur at higher states of stress. This happens to be a result of the so-called *suction hardening* often used in

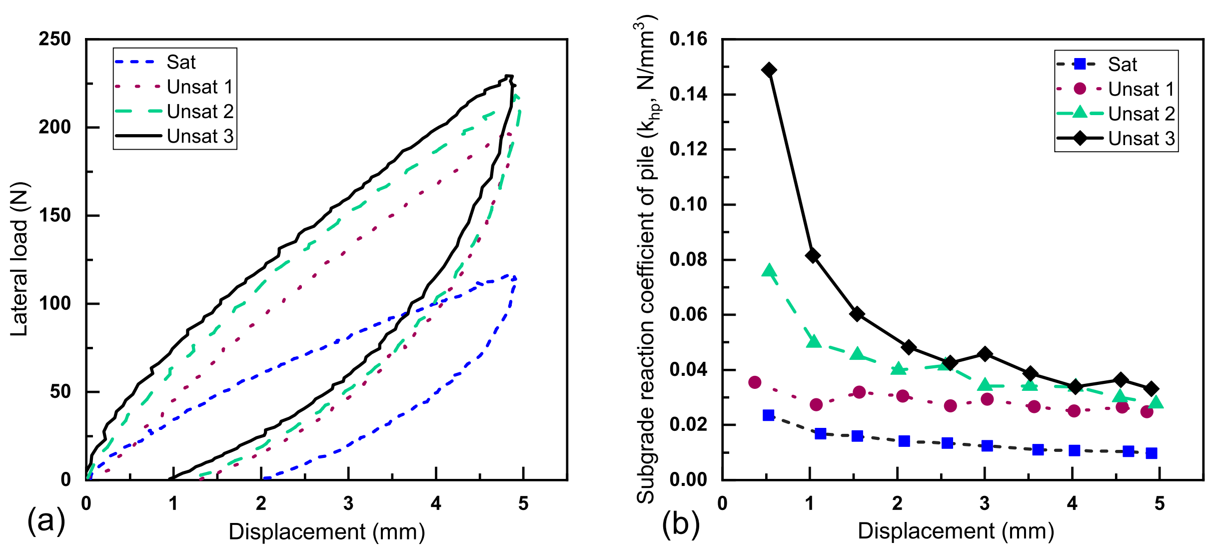

Fig. 7 Results of lateral monotonic loading tests: **a** load–displacement curves for test pile; **b** variation of subgrade reaction coefficient with the pile head displacement

conjunction with the theory of plasticity of unsaturated soils (Alonso et al. 1990).

The coefficient of lateral subgrade reaction (k_{hp}) was back-calculated from the lateral load (F) and the corresponding pile head displacement (δ) using Eqs. (4) and (5) (according to Chang 1937), in which, k_{hp} is assumed to be uniformly distributed along the pile length.

$$\delta = \frac{(1+\beta h)^3 + 0.5}{3E_pI_p\beta^3}F \tag{4}$$

where E_pI_p and h are flexural pile stiffness and load eccentricity, respectively, β is the characteristic coefficient of the pile defined by:

$$\beta = \sqrt[4]{\frac{k_{hp}D_p}{4E_pI_p}} \tag{5}$$

where D_p is the pile diameter and k_{hp} is the coefficient of horizontal subgrade reaction.

The variation of the coefficient of horizontal subgrade reaction versus pile head displacement is shown in Fig. 7b. From this figure, it is clear that for the Unsat2 and Unsat3 tests, the coefficient of horizontal subgrade reaction is characterized by an initially high value followed by a large reduction up to a displacement level of 2 mm. Beyond this level, it approaches a constant value of 0.04 N/mm^3. A relatively constant trend for k_{hp} is observed for the Unsat1 and Saturated conditions.

The results indicate that the coefficient of horizontal subgrade reaction, k_{hp}, is as low as 0.01 kN/m^3 for the saturated condition, i.e. approximately one-third that of the values obtained for the piles in unsaturated conditions. The results show that the coefficient of lateral subgrade reaction is governed by soil matric suction, which is itself a function of the degree of saturation. At large pile head displacements and in unsaturated soil conditions, k_{hp} reaches a constant value. No significant difference was observed.

3.3 Cyclic Loading

The load–displacement responses for four different cyclic loading directions, namely, two-way symmetric, two-way asymmetric, one-way, and one-way without complete unloading for the Unsat3 condition, are shown in Fig. 8. All tests exhibit a hysteretic response under cyclic unloading and reloading, implying energy dissipation in the pile-soil system. In all loading conditions, the load–displacement response of the pile in its initial loading cycle (curves in light blue) indicates an almost similar trend to that of the monotonic test. From these figures, it is obvious that the most significant variations for all loading conditions occur within their first load cycles. In the two-way loading, a gap is formed behind the pile followed by the cyclic unloading, which leads to a concave-up load–displacement curve until the pile comes back to its initial position. Subsequent cyclic loading in the opposite direction creates another gap on the other side of the pile. After completing the first cycle, separation is observed on both sides of the pile. That is the reason for the observed concave shape over the remaining cycles. It is noteworthy that such gaps have been observed and reported under field conditions (El Sharnouby and El Naggar 2012).

The cyclic secant stiffness was used to determine the stiffness degradation during the cyclic loading. The slope of the line connecting the endpoints of the load–displacement curve in each cycle obtained from cyclic loading tests was used to define the cyclic secant stiffness (Darvishi Alamouti et al. 2019; Fares-ghoshooni et al. 2021). The logarithmic expression proposed by LeBlanc et al. (2010), given by Eq. (6), was then employed to describe the progressive degradation trend:

$$\frac{k_N}{k_1} = 1 + A\ln(N) \tag{6}$$

where k_1 and k_N are the secant stiffness at the first and N-th cycles, factor A is a degradation parameter and N is the number of load cycles. Therefore, the cyclic secant stiffness acquired from each cycle was normalized by the initial secant stiffness to reveal the effect of cyclic loading on stiffness degradation. As shown in Fig. 9, for all types of loading conditions except one-way without complete unloading, stiffness degradation in the saturated soil conditions was considerably lower than those for unsaturated soil conditions. For the case of two-way loading, the stiffness of saturated soil sharply decreased during 14 load cycles where it increased slightly afterward. For all tests in the unsaturated soil conditions, the decreasing trend was observed, and the major portion of degradation occurred within the first 20 load cycles with

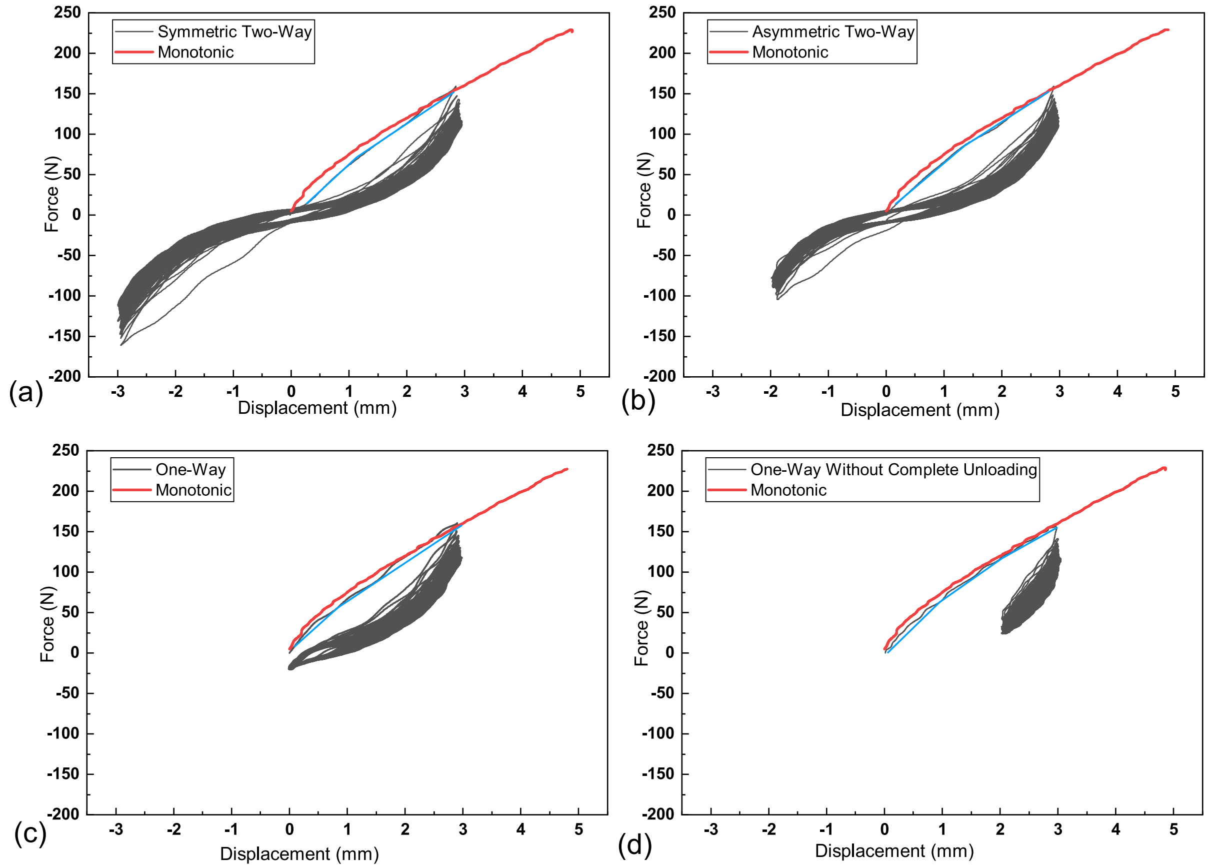

Fig. 8 Load–displacement hysteresis at the head of pile for Unsat3 tests: **a** symmetric two-way; **b** asymmetric two-way; **c** one-way; **d** one-way without complete unloading

a reduction of approximately 20%. In addition, the rate of stiffness degradation in unsaturated conditions was lower for the case of one-way without complete unloading. Degradation in unsaturated conditions followed a decreasing logarithmic trend under different cyclic loading modes. However, for the two-way loading tests carried out under saturated soil condition, the behavior was not consistent with the expected trend from Eq. (6). The stiffness reduction for both Unsat2 and Unsat3 tests was lower than Unsat1 test, which means that the matric suction has improved the resistance against stiffness degradation. The gap formation at the perimeter of the pile during the cyclic loading is believed to be the main reason for the stiffness reduction in unsaturated conditions. For the saturated condition, settlement of the sand surface around the pile was observed as shown in Fig. S1, in the supplement of this paper. This observation is attributed to sand particles flowing into the gap formed around the pile head. Further densification of this area during the cyclic loading, prevents further deterioration of the secant stiffness. One notable difference between the two-way and one-way motion is that under a two-way loading, a separation between soil and pile occurs on both sides of the pile, whereas under one-way loading, the gap develops only at one side of the pile. Therefore, the reverse component of the two-way motion can generate an additional reduction in the stiffness. Gap formation during the cyclic loading is frequently reported for piles installed in cohesive soils (Reese and Van Impe 2000; El Sharnouby and El Naggar 2012; Hong et al. 2017). Similarly, gap formation in unsaturated sandy soils may be attributed to the apparent cohesion induced by the soil matric suction. It is noteworthy that the stiffness degradation is not only dependent on the gap formation but

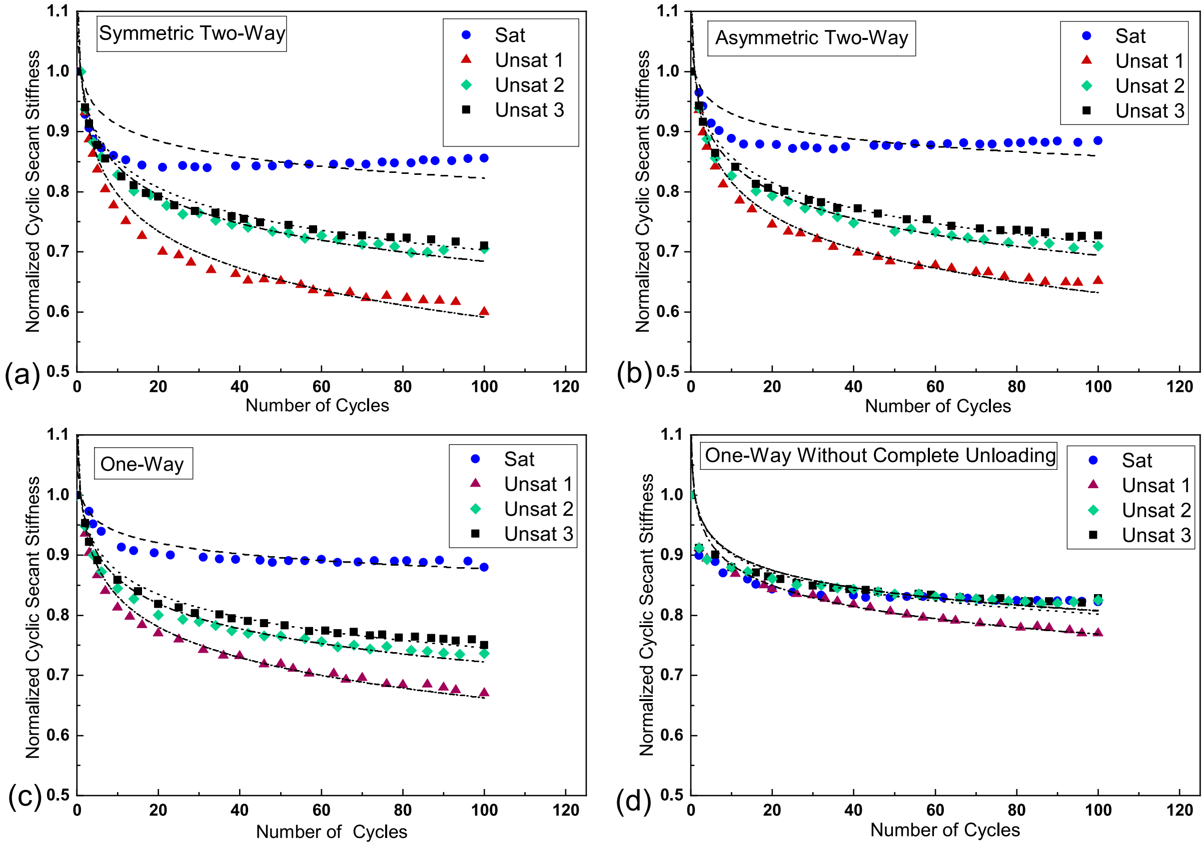

Fig. 9 Normalized cyclic secant stiffness versus number of cycles for different water-table levels (measurements and fitted relationship)

is also affected by the reduction in soil resistance during the cyclic loading. Gap formation, i.e. compression of unsaturated soils at early stages of standard cyclic tests, appears to be caused by soil volume compression around the pile. It was observed by other researchers at the initial stage of loading in unsaturated cyclic triaxial tests (Kimoto et al. 2011).

Figure 10 shows variations of the maximum pile head force with the number of cycles under different types of cyclic loading. For unsaturated conditions, cyclic loading can reduce the lateral pile capacity, and the rate of decrease becomes smaller as the cyclic loading progress. Such behavior is consistent with the cyclic triaxial tests conducted on unsaturated soils that show even under a low degree of saturation, an increase in excess pore water can gradually decreases the mean skeleton stress (Ng and Zhou 2014; Azizi et al. 2023). Nevertheless, in the 100th cycle of lateral loading, the pile in the unsaturated soil conditions had still larger lateral capacities compared to the pile embedded in the saturated soil. In these conditions, a similar response is observed for all loading cases. It can be seen that the lateral cyclic capacity of the piles in unsaturated sandy soil is not significantly influenced by the loading direction. However, there is a remarkable difference between the results obtained from different loading directions in the saturated conditions. As a result, it may be concluded that coupling behavior exists between loading directions and saturation conditions. For saturated test conditions, the formation of excess pore water pressure around the pile head can be a function of the loading direction, whereas, under unsaturated soil conditions, the gap formation behind the pile significantly governs the lateral response of the pile, resulting in the pile capacity being unaffected by the loading direction.

Under the saturated soil conditions, the least lateral capacity was observed for one-way loading without

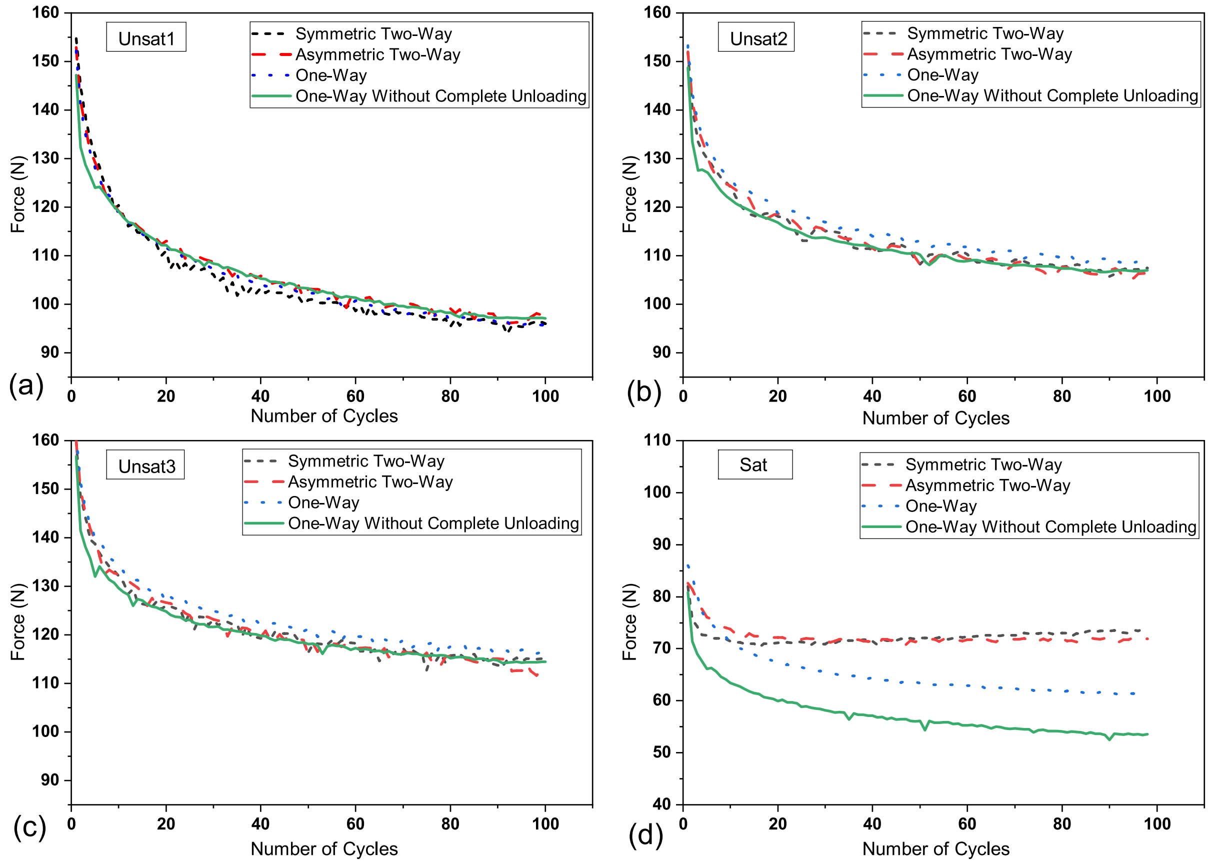

Fig. 10 Variation of lateral load at pile head with number of cycles for different water-table levels

complete unloading, reducing the lateral capacity by 22%. Under two-way loading, the lateral capacity was reduced first, followed by a mild increase in the lateral force. In all cases, the largest reduction in the lateral capacity occurred during the first 20 load cycles.

3.4 Derivation of Pile-soil Response

Various approaches have been proposed for fitting the measured bending moment profiles, including polynomial fitting and the weighted residual method (Yang and Liang 2007). In this research, a sixth-order polynomial function was employed to satisfy the best-fit curve. Such a choice is believed to be both mathematically and practically reasonable as the pressure, moment, and deflection profiles can be approximated by sufficient precision. The soil reaction profile can be back-calculated with the 2nd derivative of the bending moment with respect to the depth. As the soil pressure at the soil surface must vanish, an exponent of 2.5 was assumed (instead of 2 in the polynomial equation). According to Nip and Ng (2005), the direct derivative of the bending moment profile can intensify the measurement errors and may lead to an undesirable soil reaction profile. To overcome these shortcomings, the first and second coefficients in the polynomial were replaced by the bending moment (M_0) and the lateral load (F_0) at the soil surface. Therefore, variations of the bending moment, $M(z)$, and the soil reaction with depth, $p(z)$, can be expressed by:

$$M(z) = M_0 + F_0.z + ez^{2.5} + dz^3 + cz^4 + bz^5 + az^6 \quad (7)$$

$$p(z) = \frac{d^2M}{dz^2} = 3.75ez^{0.5} + 6dz + 12cz^2 + 20bz^3 + 30az^4 \quad (8)$$

where a, b, c, and e are constants determined from the best-fit approximation of the measured bending moment profile. Twice integration of the pile curvature (M/E_pI_p) with respect to the depth, z, yields the lateral deflection, y, along the pile length, which is given by:

$$y = \int \left(\int \frac{M}{E_pI_p} dz \right) dz \tag{9}$$

The lateral deflection profile is substantially influenced by two boundary conditions: the first condition is the pile deflection at $z = 0$ which can be calculated by means of the two LVDTs located at the pile head and the second condition is the depth of zero pile deflection. For the latter condition, some researchers assume that the pile toe is fixed. This assumption is valid when the pile is sufficiently long. To overcome this problem, the point of zero deflection is determined following an iterative procedure and satisfying compatibility between the deflection profile and the soil reaction, as explained by Choo and Kim (2016) and Li et al. (2017).

The results obtained using the procedure mentioned above for the lateral deflection and the soil reaction along the pile length are shown in Fig. 11. As clear from Fig. 11a, the soil reaction increases with the applied load, and the upper portion of the soil approaches its ultimate load, while the location of the maximum soil reaction remains unchanged during the loading process. From Fig. 11b, it may be concluded that the maximum soil reaction occurs at a depth of approximately $5D_p$ below the soil surface, regardless of saturation condition. As the WT was lowered down, the matric suction was increased, which in turn increased the mobilized soil resistance and soil reaction along the pile length while deflections were remained similar for all soil conditions. In general, the deflection of the pile decreased with the increase in depth and gradually approached zero at a point located at 300 mm below the soil surface. This length is defined as an effective pile length. The effective pile length mainly depends on the pile stiffness (Randolph 1981) and does not considerably change during the loading. Furthermore, Fig. 11c confirms that the effective pile length is not affected by the degree of saturation either.

The experimental p–y curves under saturated and unsaturated soil conditions for the monotonic and cyclic loadings are depicted in Fig. 12. These p–y curves are obtained from the last cycle of loading. Moreover, the API predictions of the p–y curves, derived from field tests performed on flexible piles, are also shown in the same figure. From this figure, it is clear that the API code shows a similar trend for both monotonic and cyclic loading, and thus it fails to

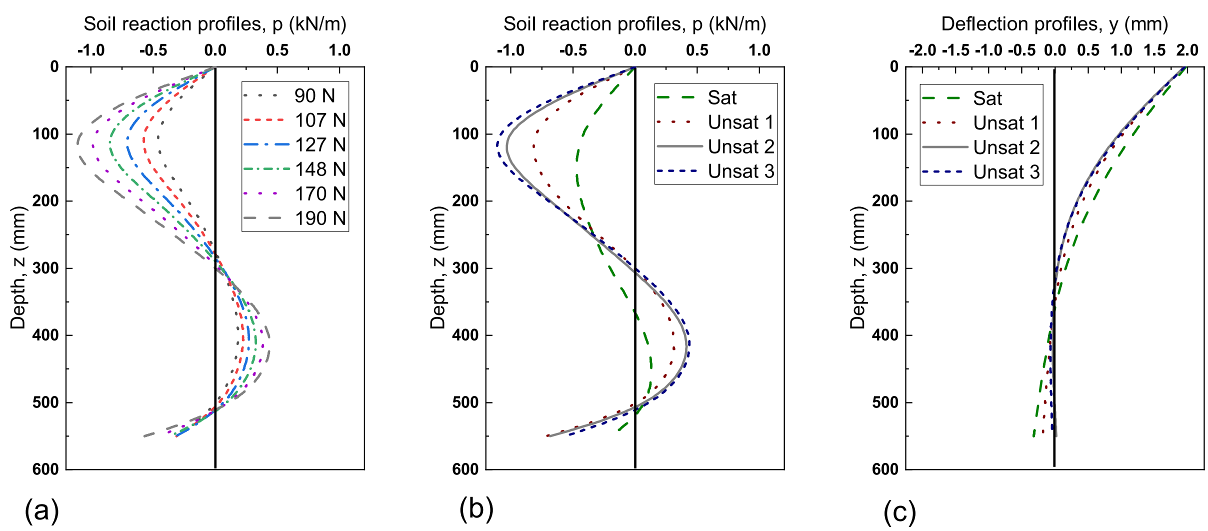

Fig. 11 Derived profiles from strain gauge measurements under monotonic loading: **a** soil reaction for different load levels (Unsat3 test); **b** soil reaction for different water table levels when pile head displacement is equal to 3 mm; **c** lateral deflection for different water table levels (pile head displacement = 3 mm)

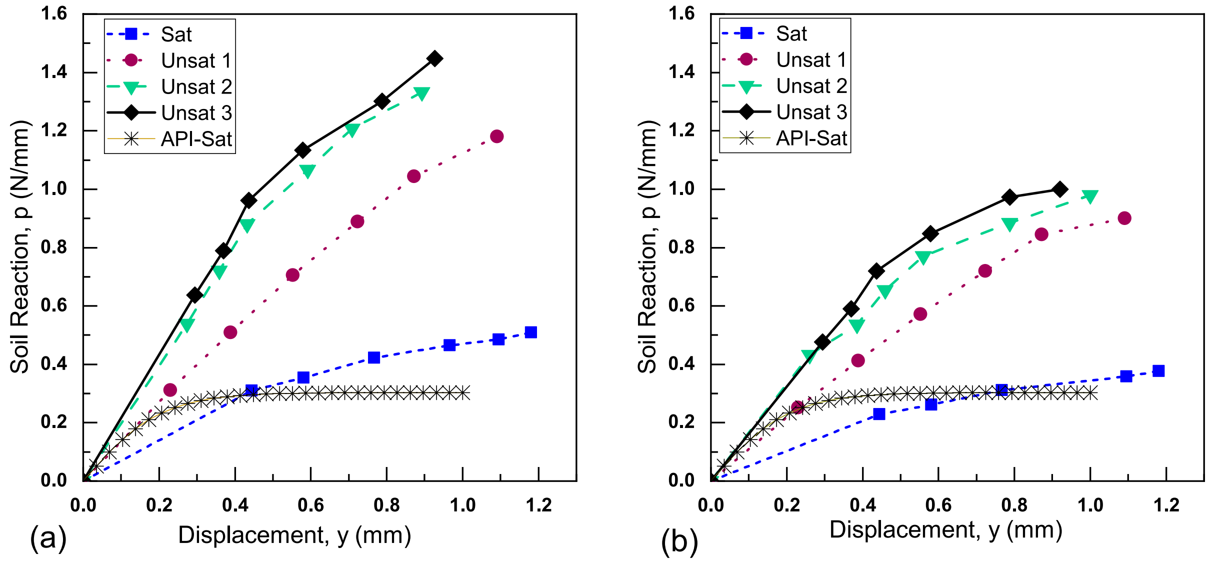

Fig. 12 Experimental p–y curves for different water table levels at depth of $4D_p$: **a** monotonic loading; **b** at 100th loading cycle

predict the cyclic behavior. It is noteworthy that the API model does not consider matric suction effects, which strongly affect the lateral loading predictions. Moreover, the API model has this limitation that the cyclic behavior of piles is not dependent on the cyclic loading characteristics such as number of loading cycles, frequency, and cyclic load ratio. These factors significantly influence pile response. It also significantly underestimates the results of tests under unsaturated soil conditions, which may lead to an uneconomical design for piles installed in the unsaturated zone. As shown in Fig. 12b, the cyclic p–y curves after 100 cycles of loading indicate that a flattening of the load–displacement curve corresponding to the ultimate soil resistance does not occur in all tests. By comparing monotonic and cyclic p–y curves, it can be observed that the soil resistance degradation under unsaturated conditions is significantly higher than that of saturated soil. This implies that the degrading cyclic factor is not constant and is affected by the degree of saturation.

3.5 Post-cyclic Behavior

The effects of previous cyclic loading on the ultimate lateral response of the pile were investigated by performing post-cyclic tests. The load–displacement behavior under post-cyclic loading and for different saturation conditions is depicted in Fig. 13. Residual forces induced during the cyclic loading phase, cause non-zero forces at the beginning of the post-cyclic loading test. Residual forces are affected by the type of cyclic loading, and in this study, the maximum residual force was observed in the one-way and one-way without complete unloading tests. A comparison between monotonic and post-cyclic loading in unsaturated conditions indicates different responses for displacement amplitudes falling within the gap zone around the pile. These differences highlight the significance of gap formation on the lateral capacity. As the pile was loaded beyond the gap zone into the relatively undisturbed region of the soil, the load–displacement curve approached the virgin monotonic loading curve and recovered its initial lateral resistance. Furthermore, the ultimate lateral resistance of the pile in the unsaturated soil conditions is unaffected by the cyclic loading history, and in the disturbed zone (gap zone), the magnitude of reduction is similar for various cyclic loading conditions. As previously explained, in saturated soil conditions, the gap formed around the pile head is filled with the loose sand from cyclic loading effects, and hence, it is observed that there is a smaller difference between the monotonic and cyclic loading results, which diminishes with the increase in the lateral loading amplitude.

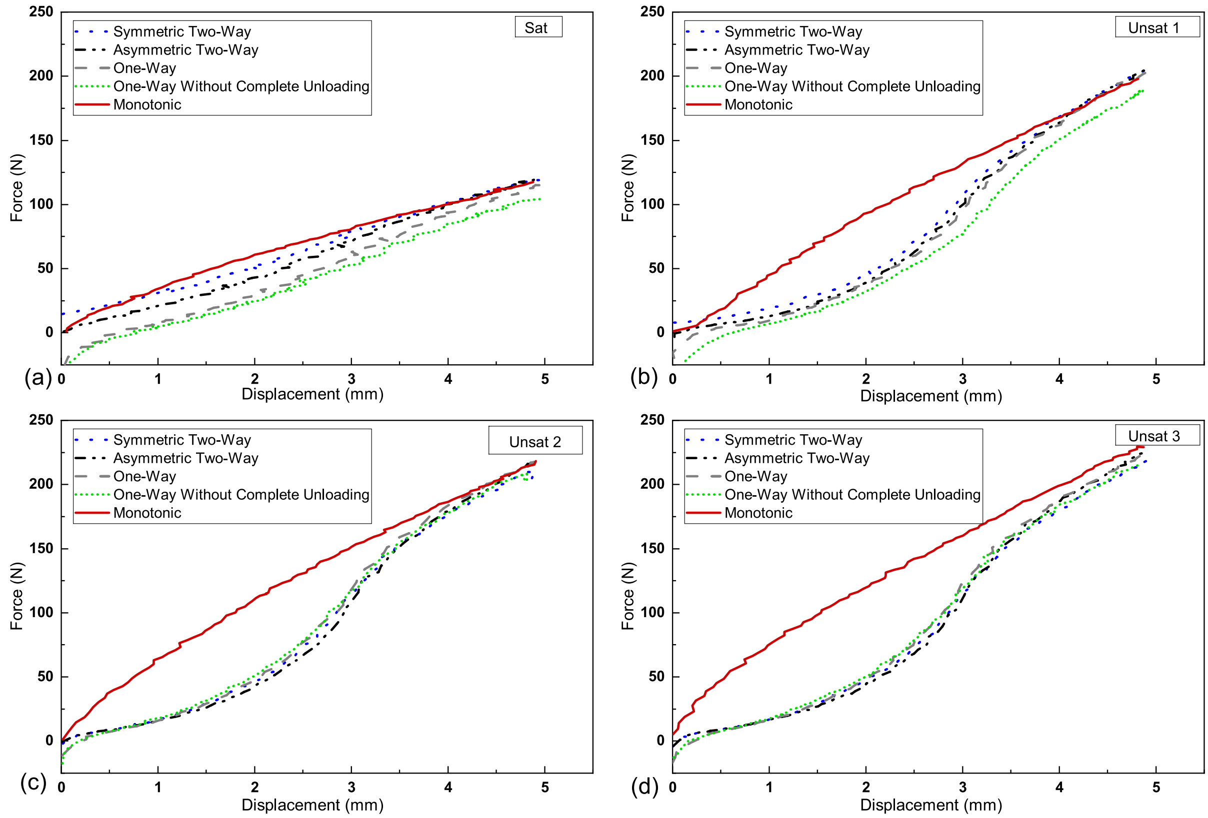

Fig. 13 Lateral load–displacement curves for post-cyclic loading

3.6 Role of Matric Suction on the Lateral Capacity

Figure 14a shows the matric suction profile under various WT scenarios based on the measurements from installed tensiometers. Matric suction profile varies nonlinearly with depth and it has larger values for deeper water tables, as expected. Apparently, the matric suction profile deviates from a linear trend which is expected and precedented in the literature as some factors may cause slight to severe nonlinearity (Al-Khazaali and Vanapalli 2019; Oh and Vanapalli 2013). In essence, when the matric suction exceeds the air entry value of the soil, the liquid phase of the soil changes from the capillary regime to the funicular and pendular regimes. In pendular regime, the water phase is no longer continuous, and this phenomenon, change of water phase from capillary to funicular and pendular regimes, results in the nonlinear variation of the matric suction with depth.

In all these scenarios, three various regimes are expected to appear along the pile length: (i) a fully saturated zone where the matric suction is zero; (ii) a capillary fringe zone where the soil is saturated but the matric suction is non-zero, and (iii) the unsaturated zone where the matric suction increases with distance above the water table. Referring to Fig. 14a and c, the state of soil near the sand surface is within the residual zone for Unsat2 and Unsat3 conditions while it is still in the transition zone for the soil condition experienced in Unsat1. That is why the degree of saturation at the soil surface for Unsat1 is significantly different from the other two cases as depicted in Fig. 6.

Lu and Likos (2006) presented the suction stress concept to describe the combined effects of the negative pore water pressure and surface tension on the effective stress and shear strength. The suction stress is defined by the inter-particle capillary forces which tend to pull the soil particles together, as follows:

$$\sigma^s = -\left(u_a - u_w\right) \text{for} u_a - u_w \leq 0 \tag{10}$$

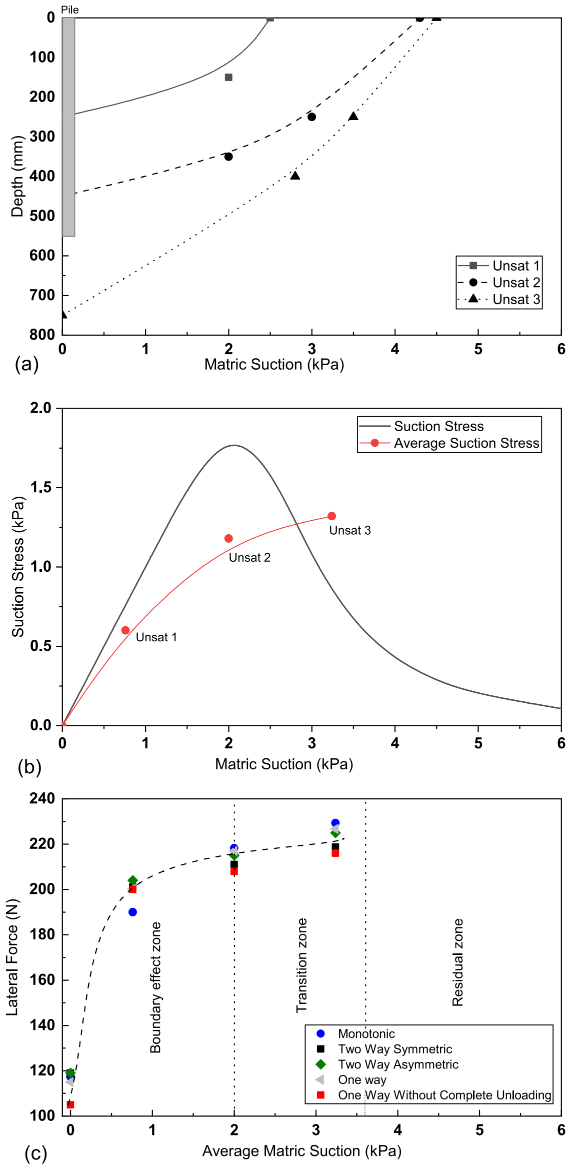

Fig. 14 **a** Matric suction profiles for various water table levels; **b** suction stress versus matric suction; **c** ultimate lateral capacity of pile for monotonic and post-cyclic loading versus average matric suction

$$\sigma^s = -\frac{(u_a - u_w)}{\left(1 + \left[B(u_a - u_w)\right]^n\right)^m} \text{for} u_a - u_w \geq 0 \tag{11}$$

Figure 14b and c show a conceptual model that relates the matric suction, the suction stress, and the ultimate lateral capacity. The suction stress increases with the increase in the matric suction and reaches its maximum value at suction corresponding to the soil air entry value. The average suction stress for each condition was also determined based on the average matric suction (i.e., abscissa of the centroid of the matric suction profile) using three mini-tensiometers and the average degree of saturation along the pile length. Figure 14c represents the ultimate lateral capacity for monotonic and post-cyclic loading at various WT depths. As clear from this figure, the ultimate lateral capacity increases nonlinearly with average matric suction in the boundary effect zone and continues with a slight increase in the transition zone. This behavior is consistent with the reported works of Vanapalli et al. (1996) who demonstrated that the contribution of the matric suction toward the shear strength, is different in transition and boundary effect zones. Beyond the air entry value, soil begins to desaturate, and the contribution of the matric suction to the elastic modulus and shear strength decreases, with increasing the matric suction. The increase in the ultimate lateral capacity with the average matric suction can be directly linked to the variation of the average suction stress (see Fig. 14b and c). Therefore, the lateral pile behavior depends on the average suction stress rather than the suction stress itself.

3.7 Modification of p–y Curve Model for Unsaturated Condition

The response of piles under lateral loading can be predicted using nonlinear soil springs. The following hyperbolic function is often utilized to describe the nonlinear features of p–y curve (Georgiadis et al. 1992):

$$p = \frac{y}{\frac{1}{k} + \frac{y}{p_u}} \tag{12}$$

where k and p_u represent the initial moduli of the subgrade reaction and ultimate lateral resistance, respectively.

In Eq. (12), no explicit parameter is present to take into account the influence of partial saturation. To overcome this handicap, a new static p–y model was developed in this study, and its performance was verified based on the lateral loading test results. The primary advantages of a modified p–y curve for unsaturated conditions are: (i) the contribution of the matric suction to the lateral resistance of piles and (ii) a more realistic prediction of the lateral pile behavior. To this end, the dependence of k and p_u on soil suction must be taken into account, as addressed subsequently.

Different methods have been proposed for predicting the ultimate lateral resistance in cohesionless soils. Zhang et al. (2005) presented a simple expression for the ultimate lateral resistance (p_u) which is expressed by:

$$p_u = \left(\eta p_{max} + \xi \tau_{max}\right) D_p \tag{13}$$

$$p_{max} = K_p^2 \gamma z \tag{14}$$

$$\tau_{max} = K \gamma z \tan \delta \tag{15}$$

where η and ξ are shape factor of pile; p_{max} = maximum earth pressure; τ_{max} = maximum side shear resistance; γ = soil unit weight; K = at-rest coefficient of earth pressure; δ = friction angle at the contact between pile and soil; $K_p = \tan^2(45 + \phi\prime/2)$, i.e., the passive earth pressure coefficient, and D_p is the pile diameter.

Lu and Likos (2004) proposed a formula for the coefficient of lateral earth pressure in unsaturated cohesionless soils as follows:

$$K_{pu} = K_p + \frac{\sigma^s\left(1 - K_p\right)}{\left(\sigma_v - u_a\right)} \tag{16}$$

where $(\sigma_v - u_a)$ is the net normal stress. It is usually assumed that the pore air pressure is continuous and connected to the atmosphere (i.e., $u_a = 0$). The ultimate lateral resistance of unsaturated cohesionless soil can be derived by substituting Eq. (16) into Eq. (14).

$$p_{u.unsat} = \left[K_p + \frac{\sigma^s\left(1 - K_p\right)}{\sigma_v - u_a}\right]^2 \eta \gamma z D_p + \xi \tau_{max} D_p \tag{17}$$

For the present study, it was found that contribution of τ_{max} to the ultimate lateral resistance is negligible (less than 4%); therefore, Eq. (17) was reduced to Eq. (18), given by:

$$p_{u.unsat} = \left[K_p + \frac{\sigma^s\left(1 - K_p\right)}{\sigma_v - u_a}\right]^2 \eta \gamma z D_p \tag{18}$$

Several researchers have shown that the horizontal modulus of subgrade reaction is governed by the elastic modulus of soil, pile flexural stiffness, and pile diameter (Phanikanth et al. 2013; Yoshida and Yoshinaka 1972). Therefore, it is important to take into account these effects when determining the horizontal modulus of subgrade reaction. The formulation proposed by Vesić (1961) considers these effects, given by:

$$k_h = 0.65\left(\frac{E_s}{1 - \nu^2}\right)\left(\frac{E_s D_p^4}{E_p I_p}\right)^{\frac{1}{12}} \tag{19}$$

where E_s and ν are the elastic modulus and Poisson's ratio of the soil, respectively. The elastic modulus plays an important role in the lateral behavior of piles and is commonly kept constant for the soil located above and below the WT, ignoring the contribution of the matric suction to the elastic modulus. To overcome this issue, the nonlinear variation of the elastic modulus with matric suction proposed by Oh et al. (2009) and expressed in Eq. (20), was adopted in this study:

$$E_{unsat} = E_{sat}\left[1 + \theta \frac{\left(u_a - u_w\right)}{\left(\frac{P_a}{101.3}\right)}\left(S^{\omega}\right)\right] \tag{20}$$

where E_{unsat} is the elastic modulus under unsaturated soil condition, E_{sat} is the elastic modulus of saturated soil, S is the degree of saturation, θ and ω are fitting parameters, and P_a is the atmospheric pressure (i.e., 101.3 kPa). The parameter θ depends on the soil type and for non-plastic coarse-grained soils, its value varies from 0.5 to 2.5 (Oh et al. 2009). The exponent ω is often taken as either 1 or 2 for coarse-grained and fine-grained soils, respectively. Therefore, θ and ω were considered equal to 0.5 and 1, respectively, for the sandy soil adopted in this investigation. Next, the value of η was adjusted to achieve the best possible match between the calculated and measured p–y curves, and a value of 2.6 was thus obtained. The saturated elastic modulus of the soil used in this research was estimated to be 3500 kPa based on the density index of 40%. Therefore, the horizontal subgrade reaction modulus for unsaturated conditions can be determined by substituting Eq. (20) in Eq. (19). Thus, using the aforementioned derivations for the horizontal modulus of subgrade reaction and the ultimate lateral resistance for piles embedded in unsaturated cohesionless soils, the modified hyperbolic relationship for the piles embedded in unsaturated cohesionless soils can be expressed as:

$$p = \frac{y}{\frac{1}{k_{unsat}} + \frac{y}{p_{u,unsat}}} \tag{21}$$

Figure 15 represents the measured p–y curves and those estimated using the modified hyperbolic model at depths of $z = 4D_p$ and $z = 8D_p$. From this figure, it is clear that there is a reasonable agreement between the measured and predicted p–y curves. Hence, it may serve as a suitable model to predict the p–y curves for piles installed in unsaturated sandy soils under monotonic loading.

4 Conclusions

In this paper, a series of lateral loading tests on piles embedded in sand were performed to investigate the influence of partial saturation on the lateral behavior of the pile-soil system. This investigation was aimed to study the load–displacement response under various loading conditions and to modify available p–y curves. The cyclic and post-cyclic responses of piles in four various loading directions were evaluated using a designed and commissioned loading device for this purpose. To consider the effects of partial saturation, different matric suction profiles were implemented by varying the water table level and studying the pile response. Moreover, experimental p–y curves were derived using the obtained bending moment profiles along the pile length. The key conclusions of this research are as follows:1.

The monotonic load–displacement of the piles indicated that an unsaturated soil condition leads to greater lateral resistance compared with the saturated soil at the same displacement level. An increase of up to 50% in the ultimate lateral resistance was observed for the cases studied.

2. The secant stiffness in unsaturated soil conditions was much higher than that in saturated conditions. However, the normalized stiffness degradation in unsaturated conditions followed a decreasing logarithmic trend under different cyclic loading modes, which is not consistent with the results from the two-way loading tests in saturated soil conditions. The opening of a gap near the pile head in unsaturated tests during the cyclic loading appears to be responsible for this significant stiffness degradation.
3. For unsaturated conditions, variations in lateral resistance during cycling loading were found to be similar for all loading directions, with most changes occurring during the first few cycles. In the saturated state, the lowermost lateral resistance was associated with the test condition of one-way without complete unloading.

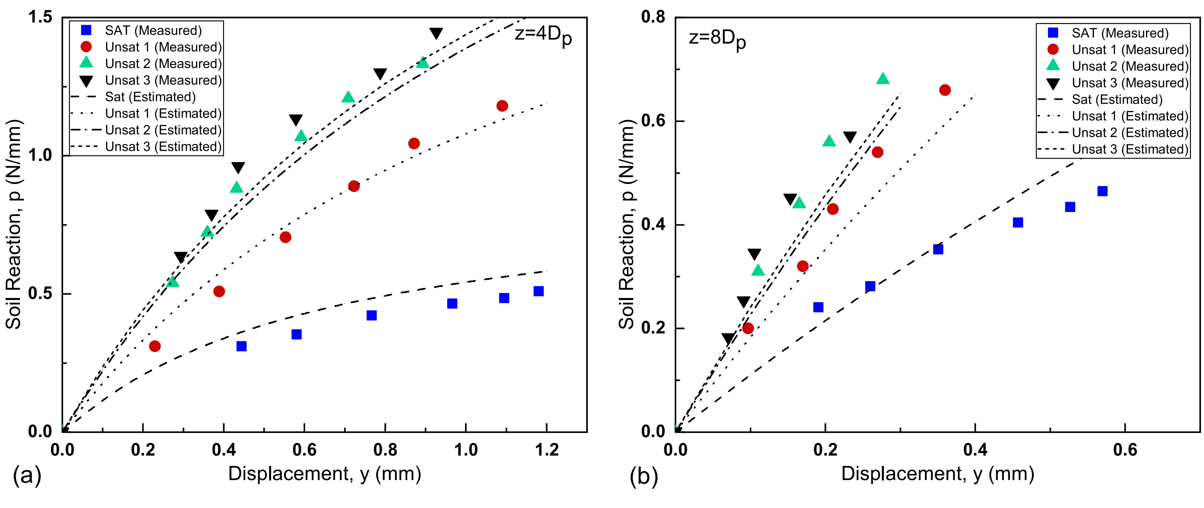

Fig. 15 Comparison of measured and estimated p–y curves for monotonic loading: **a** $z=4D_{p;}$ **b** $z=8D_p$

4. The results obtained from post-cyclic loading tests highlighted the influence of gap formation on the load–displacement response in unsaturated soils. Compared to the monotonic loading, remarkable differences in the lateral behavior of piles were observed for displacements falling within the cyclic displacement amplitudes forming the disturbed zone near the pile head. However, the ultimate lateral capacity was not affected by the previous history of cyclic loading.
5. Lowering the water table level from the soil surface resulted in a stiffer response in the monotonic as well as the cyclic p–y curves due to the contribution of suction stress to the elastic modulus and shear strength of the sand. Furthermore, the API code shows a similar trend for both monotonic and cyclic loading, and thus it fails to predict the cyclic behavior. It also significantly underestimates the results of tests under unsaturated soil conditions, which is therefore conservative and leads to uneconomical design of piles embedded in sands. To overcome this drawback, a modified p–y model was proposed to predict the lateral behavior of piles in unsaturated sandy soils, consistent with the p–y curves observed in this experimental program.

Funding The authors have not disclosed any funding.

Data Availability Enquiries about data availability should be directed to the authors.

Declarations

Conflict of Interest The authors have not disclosed any conflict of Interest.

Appendix

See Table 2.

Table 2 List of nomenclatures used in this study

Symbol	Description
$E_m I_m$	Bending stiffness of model pile
$E_n I_n$	Bending stiffness of prototype pile
F	Scale factor for length
S_e	Effective degree of saturation
S_r	Residual saturation
B, m,n	Fitting parameters of the VG model
δ	Pile head displacement
k_{hp}	Coefficient of lateral subgrade reaction
h	Load eccentricity
β	Characteristic coefficient of the pile
D_p	Pile diameter
k_N	Secant stiffness at the Nth cycles
A	Degradation parameter
N	Number of load cycles
M_0	Bending moment at the soil surface
F_0	Lateral load at the soil surface
p	Soil reaction
y	Lateral deflection
σ^s	Suction stress
u_a	Pore air pressure
u_w	Pore water pressure
p_u	Ultimate lateral resistance
η, ξ	Shape factor of pile
p_{max}	Maximum earth pressure
τ_{max}	Maximum side shear resistance
γ	Soil unit weight
K	At-rest coefficient of earth pressure
K_p	Passive earth pressure coefficient
k	Initial moduli of the subgrade reaction
E_s	Elastic modulus of the soil
ν	Poisson's ratio of the soil
E_{unsat}	Elastic modulus of unsaturated soil
E_{sat}	Elastic modulus of saturated soil
θ,ω	Fitting parameters
P_a	Atmospheric pressure

References

Abadie C (2015) Cyclic lateral loading of monopile foundations in cohesionless soils. Doctoral dissertation, Oxford University Press, Oxford, UK

Al-Khazaali M, Vanapalli SK (2019) Experimental investigation of single model pile and pile group behavior in saturated and unsaturated sand. J Geotech Geoenviron Eng 145(12):04019112. https://doi.org/10.1061/(ASCE)GT.1943-5606.0002176

Alonso EE, Gens A, Josa A (1990) A constitutive model for partially saturated soils. Géotechnique 40(3):405–430. https://doi.org/10.1680/geot.1990.40.3.405

Api R (2000) Recommended practice for planning, designing and constructing fixed offshore platforms-working stress design. API RP A 2

Arshad M, O'Kelly BC (2014) Development of a rig to study model pile behaviour under repeating lateral loads. Int J Phys Model Geotech 14(3):54–66. https://doi.org/10.1680/ijpmg.13.00015

ASTM D (2008) Standard test methods for determination of the soil water characteristic curve for desorption using a hanging column, pressure extractor, chilled mirror hygrometer, and/or centrifuge. D6836

Awad-Allah MF, Yasufuku N, Abdel-Rahman AH (2017) Cyclic response of wind turbine on piles in unsaturated sand. Int J Phys Model Geotech 17(3):161–176. https://doi.org/10.1680/jphmg.15.00017

Azizi A, Kumar A, Toll DG (2023) Coupling cyclic and water retention response of a clayey sand subjected to traffic and environmental cycles. Géotechnique 73(5):401–417. https://doi.org/10.1680/jgeot.21.00063

Basack S (2015) Design recommendations for pile subjected to cyclic load. Mar Georesour Geotechnol 33(4):356–360. https://doi.org/10.1080/1064119X.2013.778378

Basack S, Dey S (2012) Influence of relative pile-soil stiffness and load eccentricity on single pile response in sand under lateral cyclic loading. Geotech Geol Eng 30(4):737–751. https://doi.org/10.1007/s10706-011-9490-1

Basack S, Nimbalkar S (2018) Measured and predicted response of pile groups in soft clay subjected to cyclic lateral loading. Int J Geomech 18(7):04018073. https://doi.org/10.1061/(ASCE)GM.1943-5622.0001188

Basack S, Purkayastha R (2007) Behaviour of single pile under lateral cyclic load in marine clay. Asian J Civil Eng (build Hous) 8(4):443–458

Bolton M (1986) The strength and dilatancy of sands. Geotechniqué 36(1):65–78. https://doi.org/10.1680/geot.1986.36.1.65

Broms BB (1964a) Lateral resistance of piles in cohesionless soils. J Soil Mech Found Div 90(3):123–156. https://doi.org/10.1061/JSFEAQ.0000614

Broms BB (1964b) Lateral resistance of piles in cohesive soils. J Soil Mech Found Div 90(2):27–63. https://doi.org/10.1061/JSFEAQ.0000611

Chandrasekaran SS, Boominathan A, Dodagoudar GR (2010) Experimental investigations on the behaviour of pile groups in clay under lateral cyclic loading. Geotech Geol Eng 28(5):603–617. https://doi.org/10.1007/s10706-010-9318-4

Chang Y (1937) Discussion on lateral pile-loading tests by Feagin, ASCE, pp 272–278

Cheng X, El Naggar MH, Lu D et al (2022) A cyclic py elastoplastic model applied to lateral loaded pile in soft clays. Can Geotech J 60(6):885–901. https://doi.org/10.1139/cgj-2022-0314

Choi JI, Kim MM, Brandenberg SJ (2015) Cyclic p–y plasticity model applied to pile foundations in sand. J Geotech Geoenviron Eng 141(5):04015013. https://doi.org/10.1061/(ASCE)GT.1943-5606.0001261

Choo YW, Kim D (2016) Experimental development of the p–y relationship for large-diameter offshore monopiles in sands: centrifuge tests. J Geotech Geoenviron Eng 142(1):04015058. https://doi.org/10.1061/(ASCE)GT.1943-5606.0001373

Consoli NC, Diambra A, Cordeiro RE et al (2023) Field and numerical analysis of cyclic displacement controlled lateral load Tests on driven piles in a residual soil. Geotech Geol Eng 41(2):685–705. https://doi.org/10.1007/s10706-022-02295-3

Darvishi Alamouti S, Moradi M, Bahaari MR (2019) Centrifuge modelling of monopiles subjected to lateral loading. Scientia Iranica 26(6):3109–3124. https://doi.org/10.24200/sci.2018.20222

Dietrich T (1982) Incremental parabolic hardening of psammic material; Application to laterally loaded piles in sand, Deformation and failure of granular materials. Balkema, pp 13–22

El Sharnouby M, El Naggar M (2012) Field investigation of axial monotonic and cyclic performance of reinforced helical pulldown micropiles. Can Geotech J 49(5):560–573. https://doi.org/10.1139/t2012-017

Faresghoshooni A, Imam S, Mahmoodi A (2021) Model testing on the effects of section geometry and stiffness on the cyclic lateral behavior of piles in loose sand. Int J Civil Eng 19(5):563–581. https://doi.org/10.1007/s40999-020-00548-x

Frick D, Achmus M (2020) An experimental study on the parameters affecting the cyclic lateral response of monopiles for offshore wind turbines in sand. Soils Found 60(6):1570–1587. https://doi.org/10.1016/j.sandf.2020.10.004

Georgiadis M, Anagnostopoulos C, Saflekou S (1992) Centrifugal testing of laterally loaded piles in sand. Can Geotech J 29(2):208–216. https://doi.org/10.1139/t92-024

He B, Wang L, Hong Y (2017) Field testing of one-way and two-way cyclic lateral responses of single and jet-grouting reinforced piles in soft clay. Acta Geotech 12(5):1021–1034. https://doi.org/10.1007/s11440-016-0515-z

Hong Y, He B, Wang LZ et al (2017) Cyclic lateral response and failure mechanisms of semi-rigid pile in soft clay: centrifuge tests and numerical modelling. Can Geotech J 54(6):806–824. https://doi.org/10.1139/cgj-2016-0356

Huang Y, Cheng H, Osada T et al (2015) Mechanical behavior of clean sand at low confining pressure: verification with element and model tests. J Geotech Geoenviron Eng 141(8):06015005. https://doi.org/10.1061/(ASCE)GT.1943-5606.0001330

Khari M, Kassim KA, Adnan A (2013) An experimental study on pile spacing effects under lateral loading in sand. Sci World J. https://doi.org/10.1155/2013/734292

Kimoto S, Oka F, Fukutani J (2011) Monotonic and cyclic behavior of unsaturated sandy soil under drained and fully undrained conditions. Soils Found 51(4):663–681. https://doi.org/10.3208/sandf.51.663

Klinkvort RT, Hededal O, Springman SM (2013) Scaling issues in centrifuge modelling of monopiles. Int J Phys Model Geotech 13(2):38–49. https://doi.org/10.1680/ijpmg.12.00010

Komolafe O, Ghayoomi M (2023) Conceptual p–y curve framework for a single pile in cohesionless soils with variable degrees of saturation. Geotech Geol Eng 41(3):2127–2151. https://doi.org/10.1007/s10706-023-02394-9

Lalicata LM, Desideri A, Casini F (2019) Experimental observation on laterally loaded pile in unsaturated silty soil. Can Geotech J 56(11):1545–1556. https://doi.org/10.1139/cgj-2018-0322

LeBlanc C, Houlsby G, Byrne B (2010) Response of stiff piles in sand to long-term cyclic lateral loading. Géotechnique 60(2):79–90. https://doi.org/10.1680/geot.7.00196

Li W, Zhu B, Yang M (2017) Static response of monopile to lateral load in overconsolidated dense sand. J Geotech Geoenviron Eng 143(7):04017026. https://doi.org/10.1061/(ASCE)GT.1943-5606.0001698

Long J, Vanneste G (1994) Effects of cyclic lateral loads on piles in sand. J Geotech Eng 120(1):225–244. https://doi.org/10.1061/(ASCE)0733-9410(1994)120:1(225)

Lu N, Likos WJ (2004) Unsaturated soil mechanics. John Wiley & Sons Inc, Hoboken

Lu N, Likos WJ (2006) Suction stress characteristic curve for unsaturated soil. J Geotech Geoenviron Eng 132(2):131–142. https://doi.org/10.1061/(ASCE)1090-0241(2006)132:2(131)

Machmer BM (2012) Understanding the behavior of a pile foundation in unsaturated soils subjected to lateral loading. Doctoral dissertation, Clemson University

Matlock H (1970) Correlation for design of laterally loaded piles in soft clay, Offshore technology conference. OnePetro

Ng CWW, Zhou C (2014) Cyclic behaviour of an unsaturated silt at various suctions and temperatures. Geotechniqué 64(9):709–720. https://doi.org/10.1680/geot.14.P.015

Nip D, Ng CWW (2005) Back-analysis of laterally loaded bored piles. Proc Inst Civil Eng-Geotech Eng 158(2):63–73. https://doi.org/10.1680/geng.2005.158.2.63

Oh WT, Vanapalli SK (2013) Interpretation of the bearing capacity of unsaturated fine-grained soil using the modified effective and the modified total stress approaches. Int J Geomech 13(6):769–778. https://doi.org/10.1061/(ASCE)GM.1943-5622.0000263

Oh WT, Vanapalli SK, Puppala AJ (2009) Semi-empirical model for the prediction of modulus of elasticity for unsaturated soils. Can Geotech J 46(8):903–914. https://doi.org/10.1139/T09-030

Owji R, Habibagahi G, Veiskarami M (2023) Effects of cyclic and post-cyclic loading on lateral response of flexible piles embedded in dry sand. Int J Civil Eng 21(4):633–645. https://doi.org/10.1007/s40999-022-00790-5

Phanikanth V, Choudhury D, Srinivas K (2013) Response of flexible piles under lateral loads. Indian Geotech J 43(1):76–82. https://doi.org/10.1007/s40098-012-0030-6

Poulos HG, Hull TS (1989) The role of analytical geomechanics in foundation engineering, Foundation engineering: Current principles and practices. ASCE, pp 1578–1606

Randolph MF (1981) The response of flexible piles to lateral loading. Geotechnique 31(2):247–259. https://doi.org/10.1680/geot.1981.31.2.247

Rathod D, Krishnanunni K, Nigitha D (2020) A review on conventional and innovative pile system for offshore wind turbines. Geotech Geol Eng 38(4):3385–3402. https://doi.org/10.1007/s10706-020-01254-0

Reese LC, Van Impe WF (2000) Single piles and pile groups under lateral loading. CRC Press, Boca Raton

Thieken K, Achmus M, Lemke K (2015) A new static p–y approach for piles with arbitrary dimensions in sand. Geotechnik 38(4):267–288. https://doi.org/10.1002/gete.201400036

Van Genuchten MT (1980) A closed-form equation for predicting the hydraulic conductivity of unsaturated soils. Soil Sci Soc Am J 44(5):892–898

Vanapalli SK, Fredlund DG, Pufahl DE (1996) The relationship between the soil-water characteristic curve and the unsaturated shear strength of a compacted glacial till. Geotech Test J 19(3):259–268. https://doi.org/10.1520/GTJ10351J

Vesić AB (1961) Bending of beams resting on isotropic elastic solid. J Eng Mech Div 87(2):35–53. https://doi.org/10.1061/JMCEA3.0000212

Wang T, Liu W (2016) Development of cyclic p–y curves for laterally loaded pile based on T-bar penetration tests in clay. Can Geotech J 53(10):1731–1741. https://doi.org/10.1139/cgj-2015-0358

Wood DM, Crewe A, Taylor C (2002) Shaking table testing of geotechnical models. Int J Phys Model Geotech 2(1):01–13. https://doi.org/10.1680/ijpmg.2002.020101

Yang K, Liang R (2007) Methods for deriving py curves from instrumented lateral load tests. Geotech Test J 30(1):31–38. https://doi.org/10.1520/GTJ100317

Yoshida I, Yoshinaka R (1972) A method to estimate modulus of horizontal subgrade reaction for a pile. Soils Found 12(3):1–17. https://doi.org/10.3208/sandf1972.12.3_1

Zhang L, Silva F, Grismala R (2005) Ultimate lateral resistance to piles in cohesionless soils. J Geotech Geoenviron Eng ASCE 131(1):78–83. https://doi.org/10.1061/(ASCE)1090-0241(2005)131:1(78)